A Subgridding Method for the Time-Domain Finite-Difference Method to Solve Maxwell's Equations

Svetlana S. Zivanovic, Kane S. Yee, *Member, IEEE*, and Kenneth K. Mei, *Fellow, IEEE*

Abstract—**The time-domain finite-difference method (TDFDM) gives accurate results for the calculation of electromagnetic wave propagation but uses a large amount of computer memory. This paper investigates a modification to this technique that employs a variable step size. The entire computational volume is divided into a coarse grid with a large step size; a fine grid with a small step size is introduced only around discontinuities. The corresponding time increments will be related to the spatial increments with the same ratio in order to minimize the numerical dispersion. The fields within both the coarse and fine grids are found using the TDFDM while an interpolation in both space and time is utilized to calculate the tangential electric field on the coarse–fine grid boundary. This subgridding decreases the required computer memory and therefore expands the capability of the TDFDM. The technique is shown to be numerically stable, and does not entail any extra numerical error. Finally, the method is applied to the calculation of waveguides and microstrips.**

I. Introduction

In order for a numerical computation to yield accurate results the variables that are calculated should not change significantly over the linear dimension of the numerical grid. Therefore the spatial increment, Δx, used in the time-domain finite-difference method (TDFDM) [1], is taken to be much smaller than the scattering objects. Special techniques must be introduced to handle objects that are comparable to or smaller than Δx. In 1981 Holland and Simpson [2] introduced the thin-wire, thin-slot algorithm to locally modify the TDFDM. Recently, thin-wire thin gaps have been modeled with the TDFDM through the integral form of Faraday's law [3]–[5]. In all these formulations, the local field behavior is inferred from static problems. This means that in one linear dimension the thin wires or thin slots are several spatial increments long. These techniques have questionable applicability in some problems with high-power microwaves where accurate coupling calculations through small irregular holes, grooves, or slots are required. In these cases, smaller spatial increments must be used. Numerical stability then requires that the time increment also be comparably decreased. The problem becomes, at best, intolerably expensive to run if one uses a uniform time increment and, at worst, impossible to run because of the memory requirements arising from the large number of grid points.

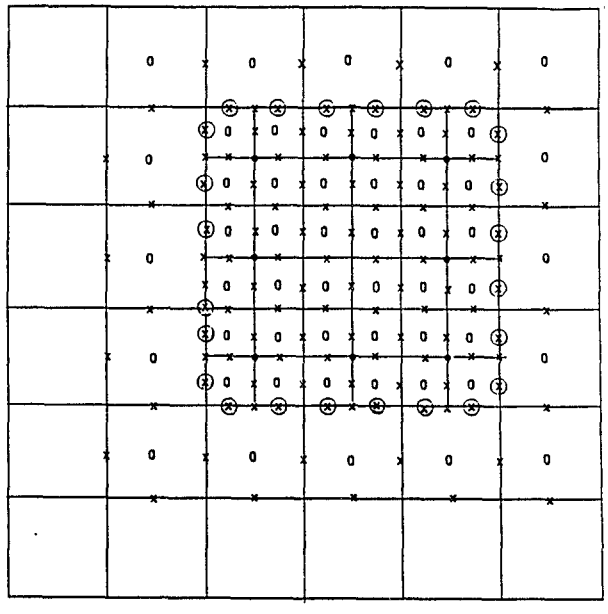

Fig. 1. Positions where the field quantities are calculated.

In 1981, Kunz and Simpson [6] introduced an expansion technique in conjunction with the TDFDM to model small local objects and demonstrated its applicability to several problems. This method requires first a calculation in a volume with a coarse grid. Spatial and time interpolations of the results from this first calculation are then used to obtain the tangential electric field components on the boundary of the subgridded volume, which are in turn used to make a second run on the subgridded volume.

The scheme investigated in this paper, the variable step size method (VSSM), also employs a variable step size. This

Manuscript received May 1, 1990; revised November 5, 1990. This work was supported by the Air Force Office of Scientific Research under Grant F19628-88-K-0025, by MICRO industrial sponsor Hughes Aircraft Company, and by the California State MICRO Program.

S. S. Zivanovic and K. K. Mei are with the Department of Electrical Engineering and Computer Sciences, University of California at Berkeley, Berkeley, CA 94720.

K. S. Yee is with the Lockheed Missile and Space Company, Palo Alto, CA 94304.

IEEE Log Number 9042343.

0018-9480/91/0300-0471$01.00 ©1991 IEEE

spatial increment is kept small around discontinuities and increased further out. Spatial and time interpolations are used to obtain the tangential electric field on the boundary between the coarse and fine grids. But instead of making two separate calculations, the calculations in the coarse grid are coupled with those in the fine grid through the use of Maxwell's equations. The close interrelations of the coarse grid and fine grid calculations will yield a more accurate modeling of the fine features within the subvolume of the coarse grid.

Fig. 1 shows a cross section of the calculational volume illustrating the positions of the tangential electric field components and normal magnetic field components. Since the spatial increment in vol. 2, the fine grid, is only half that of vol. 1, the coarse grid, the time increment for vol. 2 calculations, Δt_2, is equal to half of Δt_1, the time increment for vol. 1 calculations. This choice of spatial and time increments in the two different regions should minimize the numerical dispersion caused by the change of step size.

The fields are calculated using the TDFDM, the set of discretized Maxwell's equations:

$$H_x^{n+1/2}(i,j,k) = H_x^{n-1/2}(i,j,k) - \frac{\Delta t}{\mu}\left[\frac{E_z^n(i,j,k) - E_z^n(i,j-1,k)}{\Delta y} - \frac{E_y^n(i,j,k) - E_y^n(i,j,k-1)}{\Delta z}\right]$$

$$H_y^{n+1/2}(i,j,k) = H_y^{n-1/2}(i,j,k) - \frac{\Delta t}{\mu}\left[\frac{E_x^n(i,j,k) - E_x^n(i,j,k-1)}{\Delta z} - \frac{E_z^n(i,j,k) - E_z^n i-1,j,k)}{\Delta x}\right]$$

$$H_z^{n+1/2}(i,j,k) = H_z^{n-1/2}(i,j,k) - \frac{\Delta t}{\mu}\left[\frac{E_y^n(i,j,k) - E_y^n(i-1,j,k)}{\Delta x} - \frac{E_x^n(i,j,k) - E_x^n(i,j-1,k)}{\Delta y}\right]$$

$$E_x^{n+1}(i,j,k) = E_x^n(i,j,k) + \frac{\Delta t}{\epsilon}\left[\frac{H_z^{n+1/2}(i,j+1,k) - H_z^{n+1/2}(i,j,k)}{\Delta y} - \frac{H_y^{n+1/2}(i,j,k+1) - H_y^{n+1/2}(i,j,k)}{\Delta z}\right]$$

$$E_y^{n+1}(i,j,k) = E_y^n(i,j,k) + \frac{\Delta t}{\epsilon}\left[\frac{H_x^{n+1/2}(i,j,k+1) - H_x^{n+1/2}(i,j,k)}{\Delta z} - \frac{H_z^{n+1/2}(i+1,j,k) - H_z^{n+1/2}(i,j,k)}{\Delta x}\right]$$

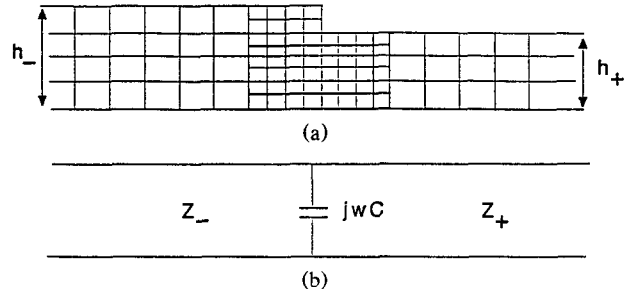

Fig. 2. (a) Two parallel plates with step discontinuity. (b) The transmission line circuit with a shunt capacitor.

$$E_z^{n+1}(i,j,k) = E_z^n(i,j,k) + \frac{\Delta t}{\epsilon}\left[\frac{H_y^{n+1/2}(i+1,j,k) - H_y^{n+1/2}(i,j,k)}{\Delta x} - \frac{H_x^{n+1/2}(i,j+1,k) - H_x^{n+1/2}(i,j,k)}{\Delta y}\right]$$

where the subscript n signifies that the quantities are to be evaluated at $t_n = n\Delta t$, and i,j,k represent the point $(i\Delta x, j\Delta y, k\Delta z)$ in the grid.

In the "interiors" of vol. 1 and vol. 2, (Fig. 1) the first three TDFDM equations are used to advance the electric field at positions marked by $\times$ and the last three to advance the magnetic field at positions marked by $\circ$. The electric field at points marked by $\times$, located on the boundary of the fine grid, are obtained through the spatial and time interpolations of the electric field at points marked by $\times$. At the beginning of each Δt the magnetic field at points marked by $\bullet$ is replaced by the space and time average of its four neighbors, calculated at the same time, in the fine grid. The tangential electric fields at the boundaries of the coarse grid are determined from the boundary conditions of the specific structure.

II. Results from Some Simple Calculations

Example 1: Two Parallel Plates with a Step Discontinuity

Fig. 2(a) shows two perfectly conducting parallel plates with a step discontinuity; Fig. 2(b) illustrates the circuit representation of Fig. 2(a), two transmission lines with an excessive fringing capacitor at the junction. The subgridded volume is over two wavelengths long, and the separation of the plates is such that only the TEM wave can propagate. For times greater than $t = 0$, a time-harmonic TEM wave is incident from the left. The TDFDM using both the uniform fine and uniform coarse grids and the VSSM are used to calculate the solution from time zero to an approximate steady state. The equivalent capacitance, C, shown in Fig. 2(b) is then calculated from the amplitude and phase of the reflected wave at a point far from the discontinuity.

Table I shows the capacitance obtained using the VSSM (column 1), the TDFDM with a uniform coarse grid (column 2), and the uniform fine grid (column 3). Column 4 is based on a quasi-static formula [7]. Except for very large step discontinuities, the VSSM improved on the accuracy of the TDFDM with a uniform coarse grid.

TABLE I
SHUNT CAPACITANCE $C \times 10^{12}$ F/m FOR THE PARALLEL PLATES SHOWN IN FIG. 2(a) AND (b) ($h_- = 1$ cm)

h_+/h_-	With Subgrid	Uniform Coarse Grid	Uniform Fine Grid	Static Approximation
0.250	5.10	5.20	5.22	5.75
0.375	3.60	3.67	3.63	3.62
0.50	2.27	2.31	2.29	2.21
0.625	1.27	1.30	1.27	1.24
0.75	0.566	0.590	0.570	0.573

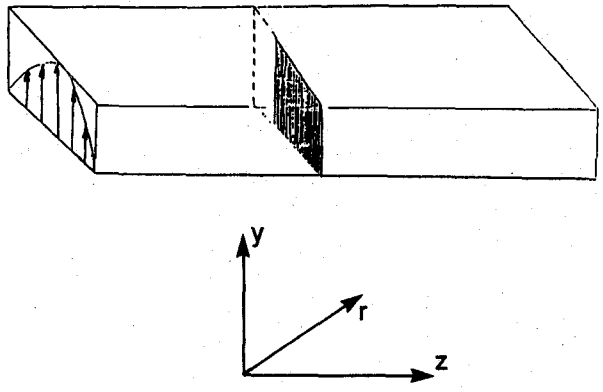

Fig. 3. A TE_{10} sinusoidal mode incident from the left (with a diaphragm).

Example 2: A Uniform Rectangular Waveguide with a Diaphragm

Fig. 3 illustrates a uniform waveguide with a diaphragm. A step harmonic TE_{10} mode of unit amplitude is incident from the left and the dimensions of the waveguide are such that only the TE_{10} mode can propagate. The problem is calculated to approximately steady state with both the VSSM and the TDFDM with a uniform coarse grid. The reflected electric fields obtained from the TDFDM and the VSSM are shown in, respectively, parts (a) and (b) of Fig. 4. The reflection coefficients are similar but there is a phase shift between the two solutions. The VSSM may have approximated the transient solution at the discontinuity better than the coarse grid.

The above examples demonstrate that subgridding does not introduce any extra numerical reflection. However, the subgridding by a factor of 2 only slightly improves the result obtained from the uniform coarse grid. By decreasing the spatial increment in the fine grid, the accuracy can be improved. In the next chapter, the spatial increment of the fine grid will be reduced to one third the spatial increment of the coarse grid in order to improve the results obtained using the TDFDM with a uniform coarse grid.

III. SUBGRIDDING USING SUBDIVISION BY A FACTOR OF 3

By decreasing the spatial increment of the fine grid, the accuracy of the technique is improved at the expense of a minimal increase in the necessary computer memory. But this increase still remains well below the memory required by the application of the TDFDM to a uniform fine grid. The tangential electric fields on the fine grid boundary are no

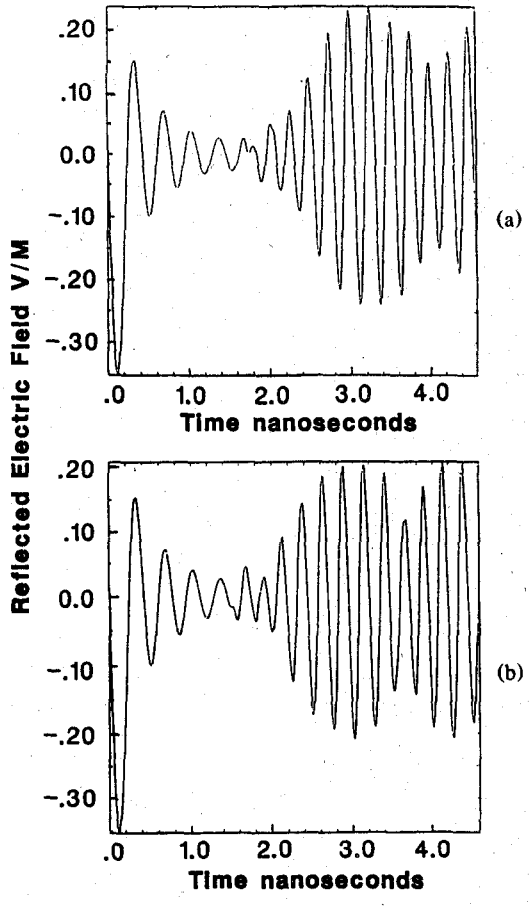

Fig. 4. Reflected electric field due to a diaphragm: (a) uniform coarse grid; (b) coarse–fine grid.

longer obtained from an average of the surrounding field points. Instead, they are calculated using a second-order equation, the homogeneous traveling wave equation:

$$\nabla^2 \boldsymbol{E} - \frac{1}{c_m^2} \frac{\partial^2 \boldsymbol{E}}{\partial^2 t} = 0$$

where c_m is the velocity of light in the medium:

$$c_m \equiv \frac{1}{\sqrt{\epsilon \mu}}.$$

This wave equation can be approximated by a second-order finite-difference wave equation (SOFDE) for each field component, and it is used to solve for the tangential electric field at the fine grid boundaries. As before, n indicates the time increment; i, j, k represent the spatial position; Δx, Δy, and

Δz are the spatial increments of the coarse grid; and Δt is the time increment of the coarse grid:

$$\begin{aligned} &\boldsymbol{E}^{n+1}(i,j,k) \\ &\quad = 2\boldsymbol{E}^{n}(i,j,k) - \boldsymbol{E}^{n-1}(i,j,k) + c_m^2 \Delta t^2 \\ &\qquad \left[\frac{\boldsymbol{E}^{n}(i+1,j,k) - 2\boldsymbol{E}^{n}(i,j,k) + \boldsymbol{E}^{n}(i-1,j,k)}{\Delta x^2} \right. \\ &\qquad + \frac{\boldsymbol{E}^{n}(i,j+1,k) - 2\boldsymbol{E}^{n}(i,j,k) + \boldsymbol{E}^{n}(i,j-1,k)}{\Delta y^2} \\ &\qquad \left. + \frac{\boldsymbol{E}^{n}(i,j,k+1) - 2\boldsymbol{E}^{n}(i,j,k) + \boldsymbol{E}^{n}(i,j,k-1)}{\Delta z^2} \right]. \end{aligned}$$

Some of the terms in the SOFDE involve fields evaluated at points external to the fine grid. Quadratic interpolation in space of the coarse grid gives a very good approximation to these field values, since the wave equation is an equation of second order. This is illustrated in Fig. 5. The fields in region 2 at points that are not located on the coarse grid (points 2, 3, 5, 6, 7, 8, 9, 10, 11, 12, 14, and 15 in the enlargement) are obtained by a quadratic interpolation of the fields at the surrounding coarse grid points. For example, the field at point 6 in the enlargement in Fig. 5 is given by (E_n referring to the electric field at point n in the enlargement)

$$E_6 = E_1 - \frac{f_x' \Delta x}{3} - \frac{f_y' \Delta y}{3} + \frac{f_x'' \Delta x^2}{18} + \frac{f_y'' \Delta y^2}{18} + \frac{f_{xy}'' \Delta x \Delta y}{9}$$

where

$$f_x' = \frac{E_{1'} - E_4}{2\Delta x}$$

$$f_y' = \frac{E_{1''} - E_{13}}{2\Delta y}$$

$$f_x'' = \frac{E_{1'} + E_4 - 2E_1}{\Delta x^2}$$

$$f_y'' = \frac{E_{1''} + E_{13} - 2E_1}{\Delta y^2}$$

$$f_{xy}'' = \frac{E_{4''} + E_{13'} - E_{1'''} - E_{16}}{4\Delta x \Delta y}.$$

(The point 1''' is located above 1' and diagonally from 1.)

The fields in region 3 (fine grid) are found using the TDFDM. The tangential electric field in region 1 is calculated from the second-order finite-difference wave equation, discussed earlier, using the corresponding tangential field values in regions 2 and 3. The normal magnetic field in region 1 is calculated using the TDFDM.

So, for every time step TDFD calculation done on the coarse grid, three calculations are done on the fine grid since the time step in the fine grid is also decreased by a factor of 3. By decreasing the fine grid step size the accuracy of the TDFDM applied to the coarse grid is improved at the expense of a minimal increase in the necessary computer memory. But this increase still remains well below the memory required by a direct application of the TDFDM. The actual amount of memory saved is, of course, dependent on the size of the discontinuities.

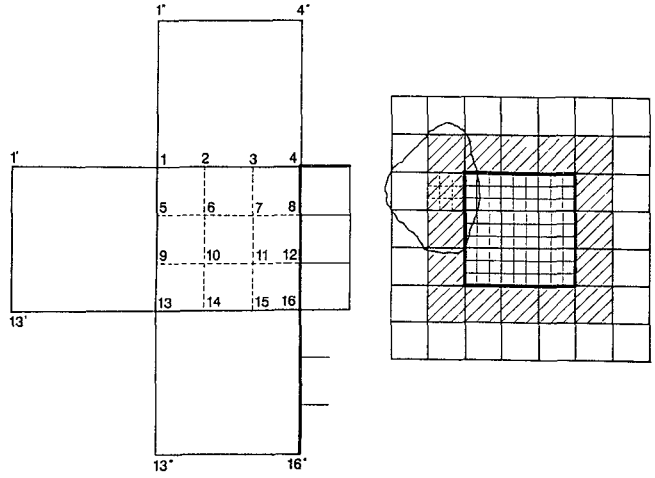

Fig. 5. Configuration used to calculate the fields in the fine mesh.
Region 1 (thick line): the fine mesh boundary.
Region 2 (shaded region, area outside region 1): coarse mesh region that borders the fine mesh region and is Δx wide, where Δx is the coarse mesh spatial increment.
Region 3 (checkered region, inside region 1): fine mesh region excluding the boundary.

A. Stability Tests of the VSSM

If the TDFDM is to have stable solutions, the time step, Δt, must satisfy the Courant stability condition [10]:

$$c_m \Delta t \leq \frac{1}{\sqrt{\frac{1}{\Delta x^2} + \frac{1}{\Delta y^2} + \frac{1}{\Delta z^2}}}.$$

In our case, $\Delta x = \Delta y = \Delta z$ and the above equation reduces to

$$c_m \Delta t \leq \frac{\Delta x}{\sqrt{3}}.$$

In all the calculations Δt and Δx were chosen to satisfy the above inequality. Since the VSSM involves different step sizes, extra numerical errors may result at the fine–coarse grid boundaries, and there is a possibility that the method could become numerically unstable after a finite number of time steps. So, to test the inherent stability of the technique, the VSSM was first used to solve for the fields in a rectangular waveguide. The waveguide was chosen because the fields can be determined analytically to any necessary accuracy, so an excellent measure of the stability and the accuracy of the technique can be obtained.

The whole waveguide was divided into a coarse grid. On the front plane the excitation equal to the exact analytic solution was applied, and the tangential electric field was set to zero on the other side surfaces.

Near the center of the waveguide, a region was further divided into a fine grid. The waveguide and grid structure used are shown in Fig. 6. The fine grid was kept small, so it was not expected that the introduction of the fine grid and consequent application of the VSSM would necessarily improve the solution in this area; instead they would just test the coarse–fine-coarse grid transitions for numerical stabil-

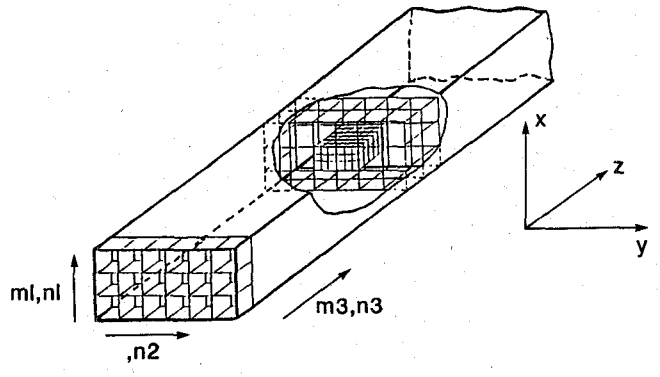

Fig. 6. Mesh structure used for stability analysis. The excitation was applied to the entire front page of the wave guide. The four sides are metal and the back face was left open. The coarse mesh used in the calculations covered the entire structure and had the dimensions $n1\Delta x \times n2\Delta y \times n3\Delta z$. The fine mesh began at the point (m_x, m_y, m_z) and had the dimensions $m1\Delta x \times m2\Delta y \times m3\Delta z$.

ity. The method was applied to a one-, a two-, and then a three-dimensional waveguide and for each case the relative errors for both the fine and coarse grids were calculated. To demonstrate numerical stability, these errors should converge, after a few time steps, to some low minimum error. Also, the relative fine grid error should be at least comparable to the coarse grid error.

The relative error over the fine grid region and the relative error at coarse grid points that coincided with fine grid points were computed for each time cycle of the excitation sine wave. The computational errors were defined as:

1) The amplitude error, E_a:

$$E_a \equiv \left| \frac{E_t - E_c}{E_t} \right| \times 100$$

where E_t is the amplitude of the exact solution for the fields and E_c is the maximum value of the calculated field over that cycle. E_a was computed for all the points in the fine grid and was then averaged.

2) The phase error, E_p, defined as the normalized time interval between the zero crossings of the calculated and the exact solutions:

$$E_p \equiv \left| \frac{\Delta t_0}{T} \right| \times 2\pi$$

where Δt_0 is the difference between the time when the exact field equals zero and when the calculated field equals zero, and T is the time period. When required, these zero crossings were determined by linear interpolation. E_p was computed for all the points in the fine grid and was then averaged.

Stability testing of the one-dimensional problem involved an excitation of $\sin \omega t$ applied at the point $z = 0$ (see fig. 6) with propagation only in the z direction and the only existing field components being E_x and H_y. The total computational domain was 100 space steps long. At $z = 50\Delta z$, four coarse grid space increments were divided into a fine grid and the fields in this region were calculated using the VSSM. After only two cycles, the relative error of the field calculation within both the coarse and the fine grid converged and steadily remained lower than 0.1%.

The problem of lowest order propagation along a two-dimensional waveguide is equivalent to the TE_{10} mode of three-dimensional waveguides, since this mode has no variation in the y direction. The excitation on the front face ($z = 0$), with the coordinate system (xz) defined in Fig. 6, was

$$E_x = \sin(\omega t)\cos(k_x x)$$

where

$$k_x = \frac{2\pi}{(n1-1)\Delta x}$$

(see Fig. 6). H_y and H_z are the only two existing components of the magnetic field. Using the notation in Fig. 6, the waveguide used in the problem had $n1 = 50$ and $n3 = 75$ ($n2 = 0$, since this is a two-dimensional problem). The calculation was performed for two different size fine grids: $m1 = 3$, $m2 = 3$ and $m1 = 6$, $m2 = 3$ and for three different frequencies, f_1, f_2, and f_3, given by

$$f_1 \equiv \frac{c}{30\Delta x}$$

$$f_2 \equiv \frac{c}{20\Delta x}$$

$$f_3 \equiv \frac{c}{15\Delta x}$$

where c is the speed of light in a vacuum (the spatial increment was arbitrary).

E_a in both the fine and the coarse grid converged to errors less than 1.5% while E_p, for all the cases, converged to values less than 0.02 rad. The relative error at the other frequencies and for the other components yielded similar results. In general, this final error (for the fine grid) decreased as the frequency was decreased from f_3 to f_2 and finally to f_1 or as the size of the fine grid region was increased.

Finally, the VSSM was applied to a three-dimensional waveguide, so all six field components were present. The excitation on the front plane was equal to a linear combination of the TE_{11} and TM_{11} modes:

$$E_x(z=0) = \left(k_y - \frac{k_x k_z}{k_{xy}^2}\right)\sin(\omega t)\sin(k_x x)\cos(k_y y)$$

$$E_y(z=0) = \left(-k_x - \frac{k_y k_z}{k_{xy}^2}\right)\sin(\omega t)\cos(k_x x)\sin(k_y y)$$

where

$$k_x = \frac{2\pi}{(n1-1)\Delta x} \qquad \text{(see Fig. 6)}$$

$$k_y = \frac{2\pi}{(n2-1)\Delta y}$$

$$k_{xy}^2 \equiv k_x^2 + k_y^2$$

$$k_z = \sqrt{\frac{\omega^2}{c^2} - k_{xy}^2}\,.$$

The dimensions of the waveguide for this calculation, using the notation in Fig. 6, were $n1 = 50$, $n2 = 50$, and $n3 = 75$. The computations were performed for two different fine grids: $m1 = 3$, $m2 = 3$, $m3 = 3$ and $m1 = 6$, $m2 = 6$,

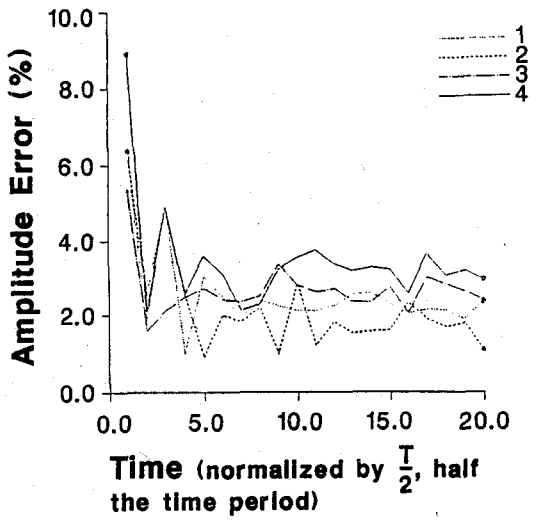

(a)

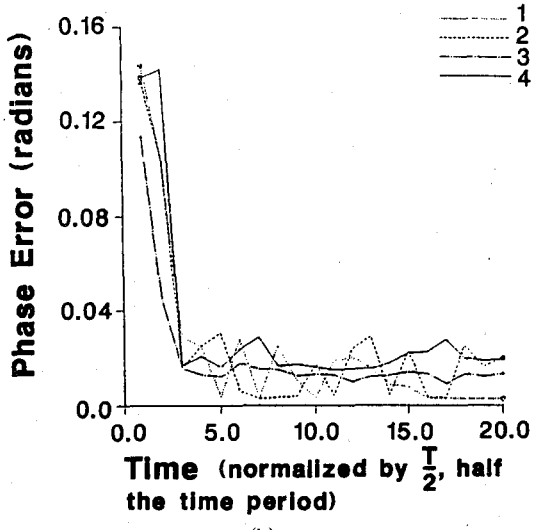

(b)

Fig. 7. (a) Comparison of the amplitude error for E_x of a three-dimensional waveguide, using a fine mesh of dimensions $3\Delta x \times 3\Delta y \times 3\Delta z$ (1. TDFDM calculation, 2. VSSM calculation) and dimensions $6\Delta x \times 6\Delta y \times 2\Delta z$ (3. TDFDM calculation, 4. VSSM calculation). (b) Comparison of the phase error for E_x of a three-dimensional waveguide, using a fine mesh of dimensions $3\Delta x \times 3\Delta y \times 3\Delta z$ (1. TDFDM calculation, 2. VSSM calculation) and dimensions $6\Delta x \times 6\Delta y \times 2\Delta z$ (3. TDFDM calculation, 4. VSSM calculation).

$m3 = 2$, as well as for the three different frequencies, f_1, f_2, and f_3, defined previously.

The relative errors of the calculated E_x for f_3 are shown in Fig. 7(a) for the amplitude error and in Fig. 7(b) for the phase error. The errors at the other frequencies tested and for the other field components exhibited similar behaviors. In general, as the frequency was increased from f_1 to f_2 and then to f_3, the final error increased and at each frequency, as the dimensions of the fine grid region were increased, the final error decreased. All the errors converged to some finite value that was slightly larger than the final error for the corresponding two-dimensional case.

Although the purpose of the above calculations was to test the stability of the method one comment can still be made about the potential accuracy of the technique. If the domain of the fine grid is small, as was the case here, the errors due to the application of the second-order difference equation dominate over any improvement that may result from the introduction of the smaller step size; hence the results are actually worse than the coarse grid calculations. But, as the domain of the fine grid is increased, the effect of these second-order errors should decrease and the fine grid results then approach and finally exceed the accuracy of the coarse grid. The results obtained in this section did show an improvement as the domain of the fine grid was increased, so the VSSM, if used properly, can improve the accuracy of the coarse grid alone.

B. Application of the VSSM to a Nondiscontinuous Microstrip

In this subsection the VSSM is used to calculate the effective dielectric constant of several different microstrips. The results are then compared with the calculations using the TDFDM as well as with other, completely different and independent techniques [11].

The effective dielectric constant, ϵ_{eff}, is often a required parameter that has to be calculated. It is a function of the applied frequency as well as of the width to height ratio and the dielectric constant, ϵ_r, of the structure. Its frequency dependence can be determined using the time dependence of the electric field at two points in the microstrip separated by a distance L in the direction of propagation.

Starting from

$$e^{-\gamma L} = \frac{E_x(\omega, z+L)}{E_x(\omega, z)}$$

where $E(\omega)$ is the Fourier transform of the time-domain electric field, $E(t)$, (the electric field calculated using the VSSM), and γ is the propagation constant:

$$\gamma = \alpha + j\beta, \qquad \beta = \frac{\omega}{c\sqrt{\epsilon_{\text{eff}}}}$$

one can determine ϵ_{eff}:

$$\epsilon_{\text{eff}} = \frac{\omega^2}{c\beta}.$$

1) Description of the Structure: The first microstrip used in the calculations, along with the grid configuration and definition of symbols, is shown in Fig. 8. Because of the symmetry of the structure, the problem is solved for only one half of the microstrip, thereby reducing the necessary computer time by a factor of 2. The whole computation region is divided into a coarse grid of dimensions $11 \times 21 \times 55\Delta z^3$, where in each case the coarse grid space step is equal to one fourth the height of the microstrip (h). The fine grid region extends the full length of the upper metal strip in the z direction, from the ground plane to about one coarse grid space step above the metal strip in the x direction, and from the center plane to several strip widths (w) out in the y direction. Typical dimensions of the fine grid region were $6 \times 9 \times 54\Delta z^3$. The boundary conditions used are the same as those in [8].

2) Electric Field Calculations: The electric field calculated using the VSSM was in very close overall agreement with the corresponding TDFDM results; the small high-frequency oscillations were somewhat different from the TDFDM computations, and even though the amplitude of these ripples was smaller than the main peak by a factor of 75, this

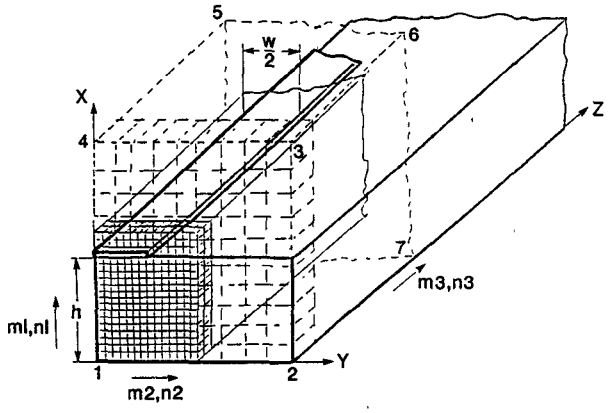

Fig. 8. Mesh structure used in the effective dielectric constant calculations. The excitation is applied to the front face (plane 1234) in the region directly below the upper metal strip. Only half the microstrip is shown here; the structure is symmetric with respect to the symmetry plane (plane 145). The upper metal strip extends the full length of the structure in the z direction. The ground plane (plane 127) extends the full length of the structure in both the y and z directions. The region between $x = 0$ and $x = h$ is filled with a dielectric. The dimensions of the coarse mesh used in these calculations are $n1\Delta x \times n2\Delta y \times n3\Delta z$. The dimensions of the fine mesh are $m1\Delta x \times m2\Delta y \times m3\Delta z$.

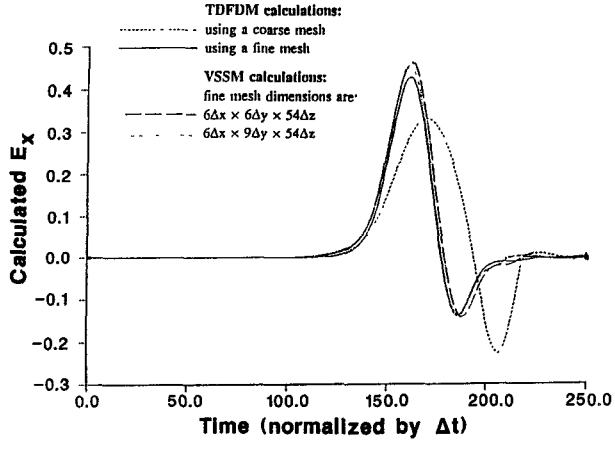

Fig. 9. Comparison of the electric field calculations obtained using the TDFDM with a coarse mesh, fine mesh and VSSM calculations using two different fine meshes.

difference was the main contributor to the discrepancies in the calculated effective dielectric constant. The VSSM was run for several different dimensions of fine grids. The calculations for E_x at $z = 22\Delta z$ for two different dimensions of fine grids, ($6\times6\times54\Delta z^3$ and $6\times9\times54\Delta z^3$) is shown in Fig. 9, along with the results using the fine grid only and the coarse grid only.

Calculations were also done for a fine grid of $9\times6\times54\Delta z^3$, but the improvement to the $6\times6\times54\Delta z^3$ size fine grid is too small to illustrate graphically; hence this result is omitted from Fig. 9. Above the metal strip there are only evanescent waves, which are less sensitive to errors in the boundary conditions. It is obvious that increasing the size of the fine grid in the x direction would not result in an appreciable improvement of the electric field. On the other hand, an increase in the y dimension of the fine grid did result in more accurate results for the fields, since there is propagation in this direction.

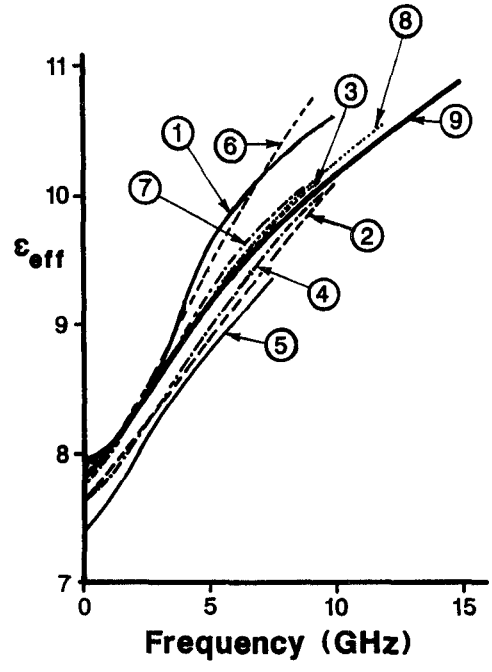

Fig. 10. Comparison of the calculated ϵ_{eff} of the microstrip as computed by various authors, with $w/h = 0.96$, $h = 3.17$ mm, and $\epsilon_r = 11.7$. Parameters are as listed above unless otherwise noted.

1) Farrar and Adams
2) Itoh and Mittra
3) Van de Capelle and Luypaert
4) Delinger
5) Schmitt and Sarges ($\epsilon_r = 11.2$)
6) Chang and Kuester
7) Pregla and Kowalski
8) Zhang, time-domain finite-difference method ($w/H = 1.0$)
9) Variable step size time-domain finite-difference method ($w/h = 1.0$)

1)–7) are taken from [8], a survey article comparing the various techniques; 8) is from [7]; 9) is the present work.

3) Calculation of the Effective Dielectric Constant of Several Microstrips: The VSSM was next applied to three different microstrips and the results are summarized below. In each case the dimensions of the coarse grid (from the notation in Fig. 8) was $n1 = 11$, $n2 = 25$, and $n3 = 55$; the fine grid dimensions (Fig. 8) were $m1 = 6$, $m2 = 9$, and $m3 = 54$.

Case 1:

$$\frac{w}{h} = 1.0 \qquad \epsilon_r = 11.7 \qquad h = 3.17 \text{ mm}.$$

The effective dielectric constant was calculated three times using three different pairs of points; each pair of points consisted of the electric field calculations at two locations on the microstrip, separated (in the z direction) by ten space steps. At each frequency the difference between the calculations of the effective dielectric constant using different pairs of points was at most 0.2. The average of the three is given in Fig. 10 along with a collection of published results [8], [10]. These published results vary greatly among each other; the VSSM calculations fall within this range and, in particular, have an acceptable agreement with the dielectric constant calculated using the TDFDM.

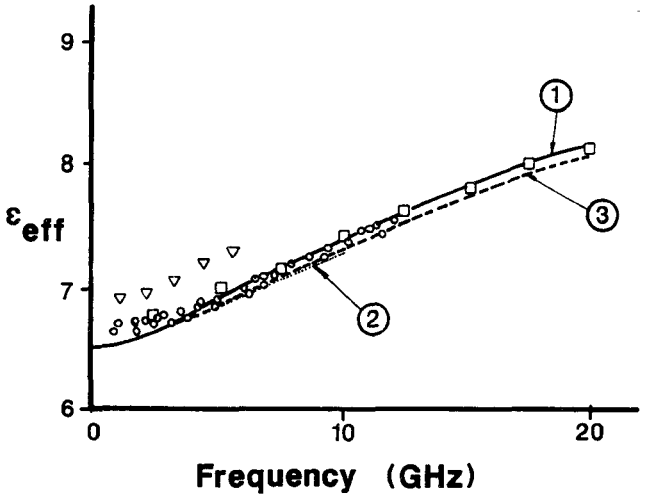

Fig. 11. Comparison of the calculated ϵ_{eff} of the microstrip as computed by various authors, with $w/h = 1.0$, $\epsilon_r = 9.7$, and $h = 1.27$ mm. Parameters are as listed above unless otherwise noted.

1) Schmitt and Sarges ($w/h = 0.96$)
2) Fujiki *et al.* ($w/h = 0.96$)
3) Kowalski and Pregla
□ Variable step size time-domain finite-difference method
▽ Deutsch and Jung ($\epsilon_r = 9.8$)
○ Hartwig *et al.* ($w/h = 0.96$).

All but □ are taken from [11], a survey article comparing the various techniques. □ is from the present work.

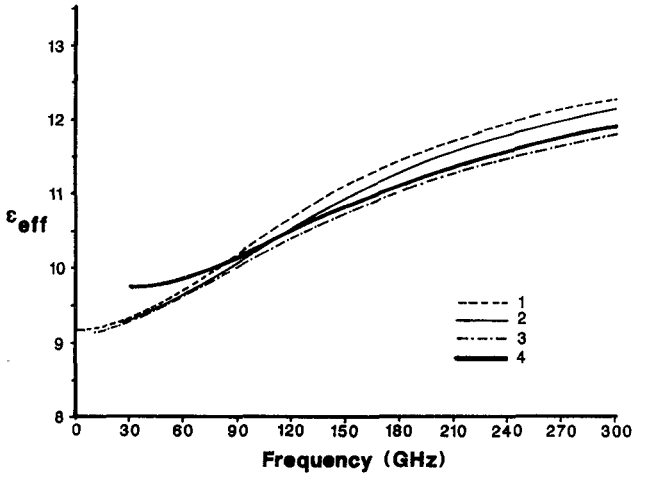

Fig. 12. Comparison of the calculated ϵ_{eff} of the microstrip as computed by various authors, with $w/h = 1.5$, $h = 0.5$ mm, and $\epsilon_r = 13.0$:

1) Edward and Owen
2) Pramanic and Bhartia
3) Zhang, time-domain finite-difference method
4) Variable step size time-domain finite-difference method.

1)–3) are taken from [7]; 4) is the present work.

Case 2:

$$\frac{w}{h} = 1.0 \qquad \epsilon_r = 9.7 \qquad h = 1.27 \text{ mm}.$$

The resulting dielectric constant (an average as before) is shown in Fig. 11, along with results from [11]. The agreement is even better than in the previous case.

Case 3:

$$\frac{w}{h} = 1.5 \qquad \epsilon_r = 13.0 \qquad h = 0.5 \text{ mm}.$$

The average calculated dielectric constant, along with the TDFDM results and the results from Edward and Owen and from Pramanic and Bhartia (all curves obtained from [8]) is given in Fig. 12. The results agree well with the three other calculations, including the TDFDM.

In summary, the dielectric constant values obtained from VSSM calculations show a good agreement with the original TDFDM results and with other independent calculations, demonstrating that the VSSM is a viable technique for determining microstrip properties.

IV. Conclusion

It has been demonstrated that the addition of the subgridding algorithm to the TDFDM produces no extra numerical reflection and yields a technique that is numerically stable. The results for the computation of the effective dielectric constant of the microstrip showed close agreement with those obtained both by the TDFDM and other independent techniques. This shows that the technique does indeed yield accurate solutions and thereby the applicability of the TDFDM is expanded. It can now be applied to a large number of structures that were difficult (if not impossible, with the current computer hardware) to treat with the ordinary TDFDM because of memory limitations.

Possible improvements to the present technique that can be investigated in the future involve testing an even smaller fine grid step size. This can involve either adding an even finer grid within the fine grid with the step size reduced by an additional factor of 3, or simply reducing the fine grid step size by an additional factor of 3. This subgridding algorithm can also be implemented in many other time-domain finite-difference codes, such as Holland's THREDE [12], Kunz's GFDTD [13], Merewether's FDTD [14], and Taflove's FDTD [15].

References

[1] K. S. Yee, "Numerical solutions of initial boundary value problems involving Maxwell's equations in isotropic media," *IEEE Trans. Antennas Propagat.*, vol. AP-14, pp. 302–307, May 1966.
[2] R. Holland and L. Simpson, "Finite-difference analysis of EMP coupling to thin struts and wires," *IEEE Trans. Electromagn. Compat.*, vol. EMC-23, pp. 88–97, May 1981.
[3] K. S. Yee, "Numerical solution to Maxwell's equations with non-orthogonal grids," in *Proc. 1st Ann. Rev. Numerical Electromagnetics Code*, Mar. 19–21, 1985.
[4] K. Umashankar, A. Taflove, B. Beker, and K. Yee, "Calculations and experimental validation of induced currents on coupled wires in an arbitrary shaped cavity," submitted to *IEEE Trans. Antennas Propagat.*
[5] A. Taflove, K. Umashankar, B. Beker, F. Harfoush, and K. Yee, "Detailed FD–TD analysis of electromagnetic fields penetrating narrow slots and lapped joints in thick conducting screens," submitted to *IEEE Trans. Antennas Propagat.*
[6] K. S. Kunz and L. Simpson, "A technique for increasing the resolution of finite-difference solution of the Maxwell equation," *IEEE Trans. Electromagn. Compat.*, vol. EMC-23, Nov. 1981.
[7] S. Ramo, J. Whinnery and T. Van Duzer, *Fields and Waves in Communication Electronics*. New York: Wiley, 1965, p. 598.
[8] X. Zhang, J. Fang, K. K. Mei, and Y. Liu, "Calculation of the dispersive characteristics of microstrips by the time-domain

finite difference method," *IEEE Trans. Microwave Theory Tech.*, vol. 36, pp. 263–267, Feb. 1988.
[9] K. K. Mei and J. Fang, "Super-absorption–A method to improve absorbing boundary conditions," submitted to *IEEE Trans. Antennas Propagat.*
[10] A. Taflove and M. E. Brodwin, "Numerical solution of steady-state electromagnetic scattering problems using the time-dependent Maxwell's equations," *IEEE Trans. Microwave Theory Tech.*, vol. MTT-23, pp. 623–630, 1975.
[11] E. F. Kuester and D. C. Chang, "An appraisal of methods for computation of the dispersion characteristics of open microstrip," *IEEE Trans. Microwave Theory Tech.*, vol. MTT-27, pp. 696–697, July 1979.
[12] R. Holland, "THREDE: A free-field EMP coupling and scattering code," *IEEE Trans. Nucl. Sci.*, vol. NS-24, Dec. 1977.
[13] K. Kunz, "General finite difference time domain," Kunz Associates, Albuquerque, NM, 1982.
[14] D. Merewether, "Finite difference solution of Maxwell's equation for EMP applications," Electro Magnetic Applications Inc., Albuquerque, NM, DNA-5301F, Apr. 1980.
[15] A. Taflove and M. E. Brodwin, "Numerical solution of steady-state electromagnetic scattering problems using the time-dependent Maxwell's equations," *IEEE Trans. Microwave Theory Tech.*, vol. MTT-23, pp. 623–630, Aug. 1975.

✠

Svetlana S. Zivanovic was born in Santa Barbara, CA, in December, 1965. She received the B.S. degree in both physics and electrical engineering from the University of California, Santa Barbara, and the M.S. degree in electrical engineering from the University of California, Berkeley. Currently, she is working towards the Ph.D. at the University of California at Berkeley. Her research interests are in radio astronomy. At present she is investigating techniques to measure and compensate for the atmospheric water vapor path delay.

Kane S. Yee (M'89) received the B.S.E.E., M.S.E.E. and Ph.D. degrees in applied mathematics from the University of California, Berkeley, in 1957, 1958 and 1963, respectively.

From 1959 to 1961, he was with the Lockeed Missiles and Space Company doing research on high-frequency asymptotic electromagnetic diffractions. From 1964 to 1966, he was employed at Lawrence Livermore National Laboratory to do work on water waves. From 1966 to 1984 he was a Professor of Mathematics and Electrical Engineering at the University of Florida and later at Kansas State University. He has been a consultant to LLNL since 1966. He rejoined the Lawrence Livermore National Laboratory in 1984. Since 1987, he has been with Lockheed Missile and Space Company in Palo Alto and Sunnyvale, CA. His research areas include electromagnetics, hydrodynamics, and numerical solutions to partial differential equations.

Dr. Yee is the author of the 1966 finite-difference time-domain electromagnetic numerical algorithm.

✠

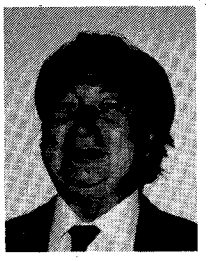

Kenneth K. Mei (S'61–M'63–SM'76–F'79) received the B.S.E.E., M.S., and Ph.D. degrees in electrical engineering from the University of Wisconsin, Madison, in 1959, 1960, and 1962 respectively.

He became a member of the faculty of the Department of Electrical Engineering and Computer Sciences of the University of California at Berkeley in 1962. He is now a professor there. His main area of interest are antennas, scattering, and numerical methods in solving electromagnetic problems.

Dr. Mei received the best paper award and honorable mention of the best paper award in 1967 and 1975 respectively from the IEEE Antennas and Propagation Society. He is a member of URSI/USNC. He served as a member of Adcomm of the IEEE Antennas and Propagation Society and as an associate editor of its TRANSACTIONS.